Molecular Phylogenetics and Evolution 65 (2012) 397–411

Contents lists available at SciVerse ScienceDirect

Molecular Phylogenetics and Evolution

journal homepage: www.elsevier.com/locate/ympev

Genealogical analyses of multiple loci of litostomatean ciliates (Protista, Ciliophora, Litostomatea)

Peter Vd'ačný [a,b,c,*], William A. Bourland [d], William Orsi [e], Slava S. Epstein [c,f], Wilhelm Foissner [b]

[a] Department of Zoology, Comenius University, Mlynská dolina B-1, SK 84215 Bratislava, Slovakia
[b] Department of Organismal Biology, University of Salzburg, Hellbrunnerstraße 34, A 5020 Salzburg, Austria
[c] Department of Biology, Northeastern University, 360 Huntington Avenue, Boston, MA 02115, USA
[d] Department of Biological Sciences, Boise State University, 1910 University Drive, Boise, ID 83725, USA
[e] Woods Hole Oceanographic Institution, 266 Woods Hole Road, Woods Hole, MA 02543, USA
[f] Marine Science Center, Northeastern University, 430 Nahant Road, Nahant, MA 01908, USA

ARTICLE INFO

Article history:
Received 3 April 2012
Revised 27 June 2012
Accepted 28 June 2012
Available online 10 July 2012

Keywords:
Body polarization
ITS1-5.8S rRNA-ITS2 region sequences
Motif
Oral simplification
Secondary structure

ABSTRACT

The class Litostomatea is a highly diverse ciliate taxon comprising hundreds of free-living and endocommensal species. However, their traditional morphology-based classification conflicts with 18S rRNA gene phylogenies indicating (1) a deep bifurcation of the Litostomatea into Rhynchostomatia and Haptoria + Trichostomatia, and (2) body polarization and simplification of the oral apparatus as main evolutionary trends in the Litostomatea. To test whether 18S rRNA molecules provide a suitable proxy for litostomatean evolutionary history, we used eighteen new ITS1-5.8S rRNA-ITS2 region sequences from various free-living litostomatean orders. These single- and multiple-locus analyses are in agreement with previous 18S rRNA gene phylogenies, supporting that both 18S rRNA gene and ITS region sequences are effective tools for resolving phylogenetic relationships among the litostomateans. Despite insertions, deletions and mutational saturations in the ITS region, the present study shows that ITS1 and ITS2 molecules can be used to infer phylogenetic relationships not only at species level but also at higher taxonomic ranks when their secondary structure information is utilized to aid alignment.

1. Introduction

Litostomateans are a highly diverse ciliate taxon comprising hundreds of species. There are two distinct lineages: free-living predators of other protists or microscopic animals and endocommensals or parasites in vertebrates (Jankowski, 2007; Lynn, 2008). These two contrasting life histories are traditionally reflected by dividing the class Litostomatea into two subclasses, the free-living Haptoria and the endocommensal Trichostomatia (e.g., Foissner and Foissner, 1988; Grain, 1994; Jankowski, 2007; Lynn and Small, 2002; Lynn, 2008). However, 18S rRNA gene phylogenies do not support this morphology-based evolutionary hypothesis (e.g., Gao et al., 2008; Pan et al., 2010; Strüder-Kypke et al., 2006; Vd'ačný et al., 2010, 2011a,b). Specifically, simple haptorians with an apically located oral opening and without a circumoral kinety, such as *Enchelys* or *Enchelydium*, were considered to be the early litostomateans (Foissner, 1984; Foissner and Foissner, 1985), while the morphologically complex dileptids were assumed as the crown litostomateans (Vd'ačný and Foissner, 2008, 2009; Xu and Foissner, 2005). Contrary to this, the 18S rRNA gene phylogenies showed that enchelyine haptorids are highly derived and their oral ciliature was very likely secondarily simplified (Vd'ačný et al., 2011a). Further, molecular analyses (Vd'ačný et al., 2010) indicated that the last common ancestor of the litostomateans was a complex ciliate with a ventrally located oral opening and complex oral ciliature, comprising a circumoral kinety (∼paroral membrane) and many preoral kineties (∼adoral organelles). Indeed, the morphologically most complex litostomateans, i.e., tracheliids and dileptids, were placed at the base of the class Litostomatea, forming a strongly supported monophylum, the subclass Rhynchostomatia, which is sister to all other litostomateans (Vd'ačný et al., 2011a,b). Another surprising finding concerned the phylogenetic position of the endocommensal Trichostomatia. They have never been depicted as a sister group of the free-living litostomateans, but have been consistently nested deep within one of the free-living litostomatean orders, the rapacious Spathidiida (Gao et al., 2008; Pan et al., 2010; Strüder-Kypke et al., 2006, 2007; Vd'ačný et al., 2010, 2011a,b). Because of these single-locus genealogical analyses and the incongruence between molecular and morphology-based approaches, there is uncertainty whether 18S rRNA molecules are elucidating the litostomatean evolution properly.

* Corresponding author at: Department of Zoology, Faculty of Natural Sciences, Comenius University, Mlynská dolina B-1, SK 84215 Bratislava, Slovakia. Fax: +421 2 60296333.
E-mail address: vdacny@fns.uniba.sk (P. Vd'ačný).

1055-7903
http://dx.doi.org/10.1016/j.ympev.2012.06.024

Therefore, we decided to study additional molecular markers, viz., the ITS region sequences to test the evolutionary trends of the litostomateans.

2. Material and methods

2.1. Collection and sample processing

Eighteen free-living litostomateans from the subclasses Rhynchostomatia and Haptoria were sampled in a variety of habitats around the world (Table 1). Species were identified using live observation, protargol impregnation, and SEM (Foissner, 1991). Seven to two hundred cells were picked with a micropipette, washed at least twice in sterile spring water to remove contaminants, and transferred into 180 µl ATL or EB buffer (Qiagen, Hildesheim, Germany). Samples were stored at +1 to +3 °C pending DNA extraction.

2.2. DNA extraction, PCR amplification, and molecular cloning

Genomic DNA was extracted according to the methods described in Vd'ačný et al. (2011a,b). The ITS1-5.8S rRNA-ITS2 region and the first two domains of the 28S rRNA gene of all species except for three (see below) were amplified by the polymerase chain reaction (PCR) using the ITS-F (5′-GTAGGTGAACCTGCGGAAGGATCATTA-3′) and LO-R (5′-GCTATCCTGAGRGAAACTTCG-3′) primers that were complementary to the conserved regions of the 3′ end of the 18S rRNA gene and the 3′ end of the D2 domain of the 28S rRNA gene (Miao et al., 2008; Pawlowski, 2000). PCR conditions and cycling parameters followed our previous protocol (Vd'ačný et al., 2011a,b). The PCR products were cloned into the vector plasmid pCR 2.1 using the TOPO TA Cloning kit (Invitrogen, Carlsbad, CA, USA). Plasmids were sequenced bi-directionally using M13 forward and reverse primers supplied with the kit at Beckman Coulter Genomics (Danvers, MA, USA).

The 18S rDNA, ITS1-5.8S rRNA-ITS2 region of *Balantidion pellucidum*, *Cultellothrix lionotiformis*, and *Microdileptus microstoma* were amplified using primers Euk A (5′-AACCTGGTTGATCCTGCCAGT-3′) and reverse primer 5′-TTGGTCCGTGTTTCAAGACG-3′ (Jerome and Lynn, 1996; Medlin et al., 1988). The ITS1-5.8S rRNA-ITS2 region for these taxa was directly sequenced with primer 1280 F (5′-TGCATGGCCGTTCTTAGTTGGTG-3′) and the reverse amplification primer (Wylezich et al., 2002) at Sequetech Corporation (Mountainview, CA, USA).

2.3. Sequence processing

Obtained sequences were imported into Chromas ver. 2.33 (Technelysium Pty Ltd.) to check for data quality and trim the 5′ and 3′ ends. The consensus sequences, based on sequences from 2 to 12 clones (Table 1), were created in BioEdit ver. 7.0.5.2 (Hall, 1999) with an inclusion threshold frequency of 80% identity.

The boundaries of the ITS1 and 5′ end of the 5.8S rRNA gene were identified by comparison with the sequences available in GenBank via the Rfam database available on the web page

Table 1
Characterization of new ITS1-5.8S rRNA-ITS2 region sequences of 18 litostomatean ciliates (arranged alphabetically).

Taxon	Collection site	Culture conditions[a]	No. of cells picked	No. of clones sequenced	Sequence length (nt)	GC content (%)
Apobryophyllum schmidingeri Foissner and Al-Rasheid, 2007	Germany, terrestrial mosses	NFP	30	10	368	32.3
Apodileptus visscheri rhabdoplites Vd'ačný and Foissner, 2012[b,c]	Salzburg, Austria, ephemeral pond	NFP	50	11	363	36.4
Arcuospathidium namibiense tristicha Foissner et al., 2002	Germany, terrestrial mosses	NFP	15	2	368	34.8
Arcuospathidium sp.[d]	Australia, leaf litter	NFP	70	12	368	35.9
Balantidion pellucidum Eberhard, 1862[e]	Boise, Idaho, USA, garden water tank	ES	20	–	393	36.4
Cultellothrix lionotiformis (Kahl, 1930) Foissner, 2003[e]	Pyhätunturi mountain, Finland, terrestrial mosses	NFP	20	–	372	34.4
Dileptus costaricanus Foissner, 1995	Botswana, floodplain soil	NFP	10	10	369	34.1
Enchelyodon sp.[d]	Boise, Idaho, USA, floodplain soil	NFP	50	9	364	36.5
Enchelys gasterosteus Kahl, 1926	Jamaica, bromeliad tank	ES	10	11	369	37.7
Microdileptus microstoma (Vd'ačný and Foissner, 2008) Vd'ačný and Foissner, 2012[e,f]	Boise, Idaho, USA, floodplain soil	NFP	30	–	313[g]	36.1
Monomacrocaryon terrenum (Foissner, 1981) Vd'ačný et al., 2011[h]	Upper Austria, soil	NFP	200	12	372	34.7
Protospathidium muscicola Dragesco and Dragesco-Kernéis, 1979	Botswana, floodplain soil	NFP	35	11	362	29.6
Pseudomonilicaryon fraterculum Vd'ačný and Foissner, 2012[c]	Boise, Idaho, USA, floodplain soil	NFP	15	9	367	33.2
Rimaleptus mucronatus (Penard, 1922) Vd'ačný et al., 2011	Boise, Idaho, USA, floodplain soil	NFP	70	12	371	35.3
Semispathidium sp.[d]	NP Krüger, South Africa, floodplain soil	NFP	18	11	368	36.7
Spathidium sp.[d]	Boise, Idaho, USA, floodplain soil	NFP	8	11	368	34.8
Trachelius ovum (Ehrenberg, 1831) Ehrenberg, 1833	Salzburg, Austria, University pond	ES	7	12	362	31.2
Trachelophyllum sp.[d]	Boise, Idaho, USA, floodplain soil	NFP	20	12	363	33.3

[a] ES, environmental sample; NFP, non-flooded Petri dish culture, as described in Vd'ačný and Foissner (2012).
[b] Designated as *Dileptus* cf. *jonesi* in Vd'ačný et al. (2011a,b).
[c] The original description will be published in our monograph on dileptids. To avoid nomenclatural problems we disclaim those names for nomenclatural purposes (Article 8.3 of the ICZN, 1999).
[d] These species are new and their descriptions are in preparation.
[e] PCR products sequenced directly.
[f] Designated as *Rimaleptus microstoma* in Vd'ačný et al. (2011b).
[g] Partial sequence.
[h] Designated as *Monomacrocaryon terrenus* in Vd'ačný et al. (2011a,b).

http://www.sanger.ac.uk/Software/Rfam/ (Griffiths-Jones et al., 2005). The boundaries of ITS2 were determined using the ITS2 Annotation feature of the ITS2 database (http://its2.bioapps.biozentrum.uni-wuerzburg.de) (Koetschan et al., 2010), which recognizes the ITS2 proximal stem, i.e., a hybridized 5.8S-28S rRNA fragment forming a characteristic approximately 15 bp-long imperfect helix (Keller et al., 2009).

2.4. Predicting secondary structures of ITS1 and ITS2 molecules

The consensus sequences of the litostomatean ITS1 and ITS2 regions were aligned by the ClustalW algorithm implemented in the program Clustal X ver. 2.0.12 (Larkin et al., 2007) with arbitrarily chosen parameters (8.0 for gap opening penalty and 6.0 for gap extension penalty). The consensus ITS1 and ITS2 secondary structures were predicted from the ITS1 and ITS2 alignment, respectively, using the RNAalifold WebServer (http://rna.tbi.univie.ac.at/cgi-bin/RNAalifold.cgi) with default options (Bernhart et al., 2008; Gruber et al., 2008). With the guidance of these consensus structures, the secondary structures of ITS sequences were predicted with Mfold (http://mfold.bioinfo.rpi.edu/cgi-bin/rna-forum1.cgi) by screening for thermodynamically optimal and suboptimal secondary structures using the default values (Zuker, 2003). Results for all studied litostomatean species were compared to reveal the folding pattern common to all of them. Subsequently, we have established conserved structural models for litostomateans in order to reveal evidence of homology useful for aiding alignments. The base frequency at each position and mutual information of base-paired regions were calculated using the program RNA Structure Logo (http://www.cbc.dtu.dk/~gorodkin/appl/slogo.html) (Gorodkin et al., 1997). For each structural domain, the number of base pairs, unpaired bases in bulges and interior loops were investigated and compared. If different nucleotides occurred at the same position of an ITS structural domain, they were encoded in motifs according to the NCBI webpage (www.ncbi.nlm.nih.gov/blast/fasta.shtml).

2.5. Sequence alignments and phylogenetic analyses

To determine the genealogical relationships among litostomateans, we analyzed eleven alignments (Table 2) comprising up to 23 in-group taxa (Table 3). Outgroup sequences were not included because it was not possible to obtain an unambiguous alignment with either armophorean and/or spirotrichean sequences. The litostomatean 18S rRNA sequences were aligned in the ARB-package (Ludwig et al., 2004), while Clustal X (Larkin et al., 2007) was used to align the ITS sequences. The resulting alignments were manually edited in the program BioEdit (Hall, 1999), according to the secondary structural features of the 18S rRNA molecule as predicted by the ARB-package, and the ITS molecules proposed in this study. Ambiguously aligned and hyper-variable regions were eliminated.

All alignments were analyzed with three phylogenetic methods: Bayesian inference (BI), maximum likelihood (ML), and maximum parsimony (MP). Bayesian inference analyses were performed with the program MrBayes (Ronquist and Huelsenbeck, 2003), using the

Table 2
Comparison of alignments and tree statistics for MP analyses.

Dataset	No. of taxa	No. of characters	No. of parsimony informative characters	No. of variable characters	Length of tree	CI	CIex	RI	RC
5.8S	23	150	29	12	105	0.5333	0.4615	0.6755	0.3603
5.8S (by eye exclusion)	23	144	23	12	68	0.6176	0.5185	0.7679	0.4743
ITS1	22	135	77	14	282	0.5390	0.5076	0.6049	0.3260
ITS1 (by eye exclusion)	22	98	55	10	180	0.5500	0.5207	0.6368	0.3502
ITS2	23	114	52	22	284	0.4577	0.3984	0.5587	0.2558
ITS2 (by eye exclusion)	23	99	43	18	232	0.4612	0.4048	0.5690	0.2624
ITS1 + 5.8S + ITS2	22	399	158	47	696	0.4813	0.4333	0.5482	0.2639
ITS1 + 5.8S + ITS2 (by eye exclusion)	22	341	121	39	499	0.4910	0.4393	0.5767	0.2831
18S	22	1493	84	60	234	0.7265	0.6168	0.8118	0.5897
18S + ITS1 + 5.8S + ITS2	22	1832	202	99	717	0.5704	0.4909	0.6578	0.3752
18S + ITS1 + 5.8S + ITS2 + 5′ end 28S	15	2310	328	114	1016	0.6171	0.5624	0.6853	0.4229

CI, consistency index; CIex, consistency index excluding uninformative characters; RI, retention index; RC, rescaled consistency index.

Table 3
List of ciliate taxa with GenBank accession numbers of corresponding 18S rRNA gene sequences and ITS1-5.8S rRNA-ITS2 region sequences included in the phylogenetic analyses. Sequences obtained during this study are in bold.

Taxon	GB number		Taxon	GB number	
	18S	ITS region		18S	ITS region
Apobryophyllum schmidingeri	JF263441	**JX070870**[a]	*Lacrymaria marina*	DQ777746	DQ811088
Apodileptus visscheri rhabdoplites	HM581678	**JX070869**[a]	*Microdileptus microstoma*	HM581678	**JX070866**[b]
Arcuospathidium namibiense tristicha	JF263442	**JX070872**[a]	*Monomacrocaryon terrenum*	HM581674	**JX070864**[a]
Arcuospathidium sp.	JF263443	**JX070871**[a]	*Protospathidium muscicola*	JF263449	**JX070876**[a]
Balantidion pellucidum	JF263444	**JX070880**	*Pseudomonilicaryon fraterculum*	HM581677	**JX070867**[a]
Balantidium coli of ostrich origin	AM982723	AM982726	*Rimaleptus mucronatus*	HM581675	**JX070865**[a]
Balantidium coli of pig origin	AM982722	AM982724	*Semispathidium* sp.	JF263450	**JX070873**[a]
Cultellothrix lionotiformis	JF263445	**JX070879**	*Spathidium* sp.	JF263451	**JX070877**[a]
Dileptus costaricanus	HM581679	**JX070868**[a]	*Trachelius ovum*	HM581673	**JX070863**[a]
Enchelyodon sp.	JF263446	**JX070874**[a]	*Trachelophyllum* sp.	JF263452	**JX070878**[a]
Enchelys gasterosteus	JF263447	**JX070875**[a]	*Troglodytella abrassarti*	AB437346	EU680313
Epispathidium amphoriforme	DQ411857	AF223570			

[a] These new sequences also include first two domains of the 28S rRNA gene.
[b] ITS1 sequence is partial.

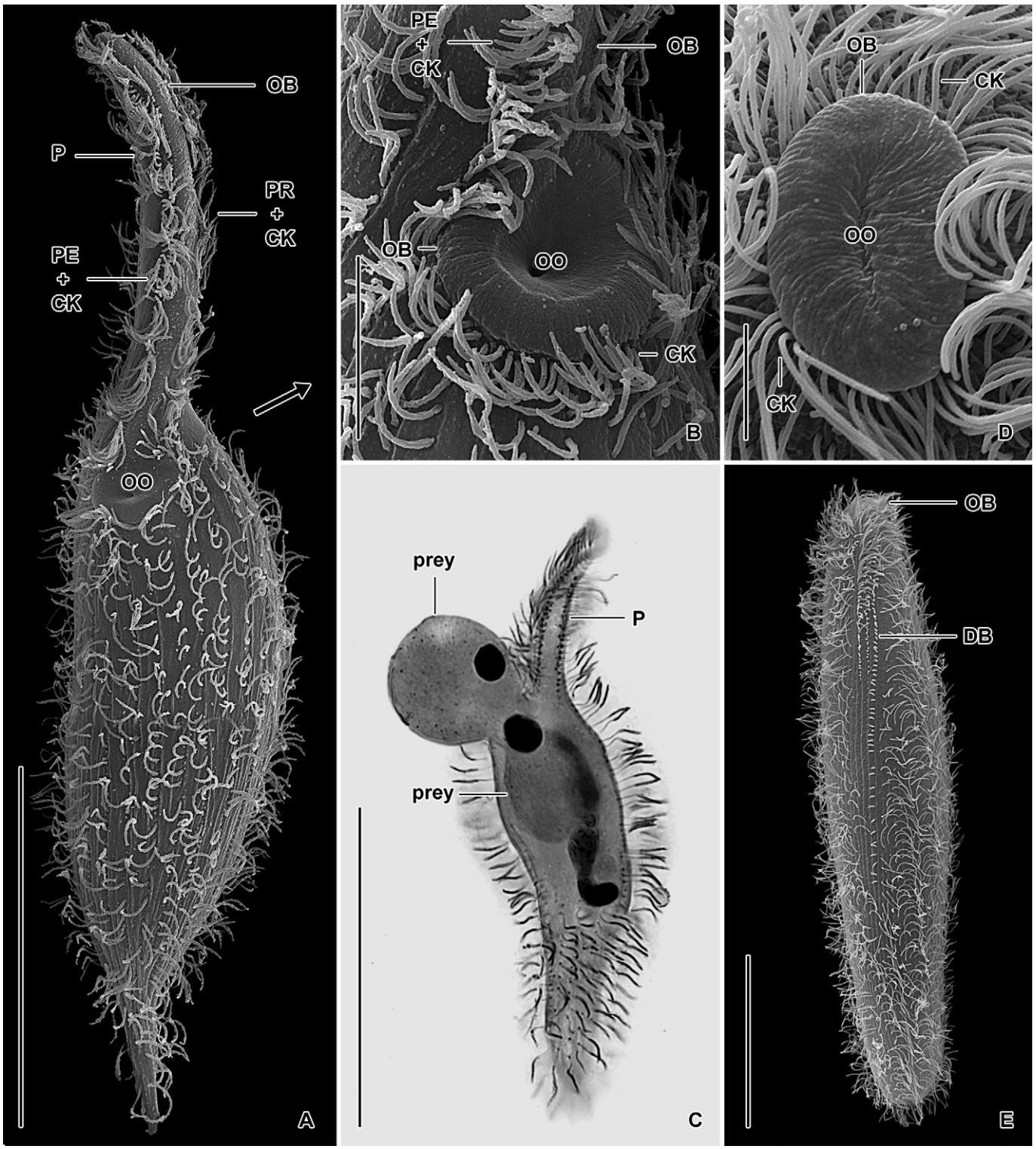

Fig. 1. Morphological diversity and food uptake in free-living litostomatean ciliates after protargol impregnation (C) and in the scanning electron microscope (A, B, D–J). From Foissner et al. (1995) (F, G), Foissner et al. (1999) (H, I); Vd'ačný and Foissner, 2012 (A–C); and originals (D, E, J). (A, B) *Apodileptus visscheri rhabdoplites*, ventral view showing the narrow body with the oral opening at the base of the proboscis (B). (C) *Microdileptus breviproboscis*, lateral view of a specimen engulfing a dividing naked amoeba. (D, E, J) *Enchelyodon* sp., frontal view of oral bulge in the centre of which is the oral opening (D), dorsal overview showing the apically located oral apparatus and the dorsal brush, a special field of short bristles of unknown function (E), and dorsolateral view showing a specimen ingesting a large prey ciliate (J). (F, G) *Litonotus varsaviensis*, lateral overview showing the unciliated left side, the vaulted dorsal side bearing a dorsal brush, and the slit-like oral apparatus (arrowheads) extending on the narrow ventral side. The anterior body third opens widely during feeding (G), causing pleurostomatids to resemble simple polar haptorids although their oral bulge extends far posteriorly. (H, I) *Monodinium balbianii balbianii*, representative specimen showing the anterior oral dome at the top of which is the oral opening. In *Monodinium* the ciliature is reduced to an anterior girdle (H). The oral opening can open widely during feeding because the prey (*Tetrahymena*) is ingested whole (I). CG, ciliary girdle; CK, circumoral kinety; DB, dorsal brush; OB, oral bulge; OC, oral ciliature; OO, oral opening; P, proboscis; PE, perioral kinety; PR, preoral kineties. Scale bars: 5 μm (D), 10 μm (B), 25 μm (H, I), and 50 μm (A, C, E, F, G, J).

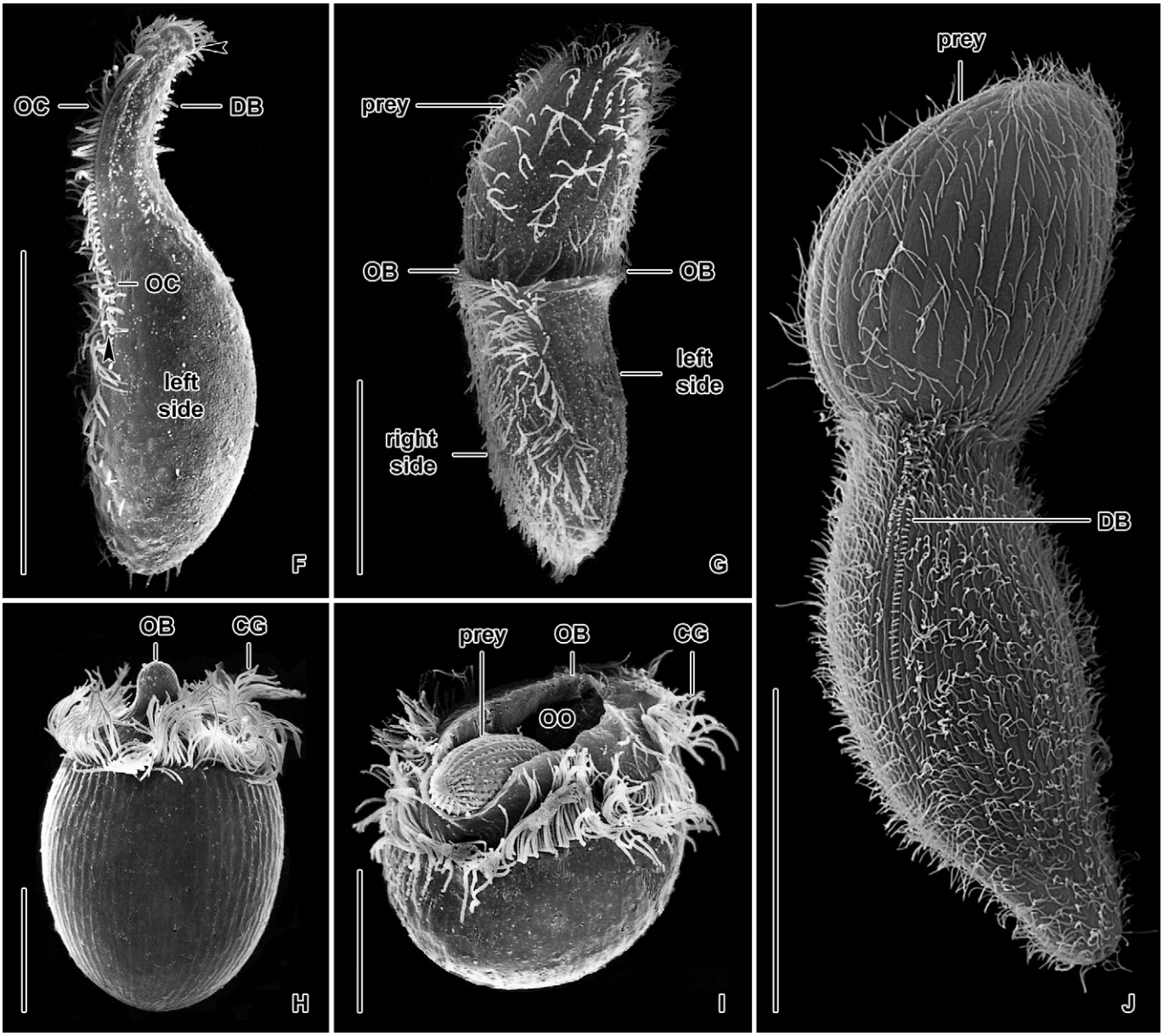

Fig. 1 (*continued*)

nucleotide substitution models determined by the program jModelTest ver. 0.1.1 (Posada, 2008) under the Akaike Information Criterion for each alignment (Table 4). Four simultaneous MCMC chains were run for 5,000,000 generations with trees sampled every 1000 generations. The first 25% of sampled trees were considered as burn-in and discarded prior tree reconstruction. A 50% majority rule consensus of the remaining trees was used to calculate posterior probabilities (PP) of the branching pattern. The ML analyses were computed on the CIPRES Portal (http://www.phylo.org), using RAxML with settings as described in Stamatakis et al. (2008). The MP trees were constructed using PAUP* ver. 4.0b8 with randomly added species (10 replications) and tree bisection–reconnection (TBR) branch-swapping algorithm in effect (Swofford, 2003). The reliability of the ML and MP trees was tested by the bootstrap approach, using 1000 pseudoreplicates and a heuristic search algorithm. Support values from all tree-building methods were annotated onto the tree topology having the best log-likelihood score.

2.6. Constrained analyses

Constrained analyses were carried out on the 18S + ITS1 + 5.8S + ITS2 + 5′ end 28S dataset in which the family Dileptidae was forced to be monophyletic, and on the 18S + ITS1 + 5.8S + ITS2 dataset where a sister relationship was forced for the subclasses Haptoria and Trichostomatia. Constrained trees were built in PAUP*, using ML criterion and heuristic search with TBR swapping algorithm and 10 random sequence addition replicates. The site-wise likelihoods for the best unconstrained ML trees and all constrained trees were calculated in PAUP* under the substitution models with parameters as suggested by jModeltest (see above and Table 4). The reliability of the constrained trees was analyzed through the approximately unbiased test (AU) and the Shimodaira–Hasegawa test (SH) implemented in the CONSEL software package (Shimodaira and Hasegawa, 2001).

Table 4
Summary of nucleotide substitution models selected for 11 datasets under the Akaike Information Criterion in jModeltest ver. 0.1.1.

Dataset	DNA substitution model	No. of substitution types (nst)	Invariant sites (I)	Gamma shape (Γ)
5.8S	TVMef	6	Yes (0.5780)	0.5800
5.8S (by eye exclusion)	TVM	6	No	0.1230
ITS1	TrN	6	Yes (0.1560)	1.3400
ITS1 (by eye exclusion)	HKY	2	Yes (0.1890)	1.4220
ITS2	TIM2	6	No	0.3980
ITS2 (by eye exclusion)	TIM2	6	No	0.3070
ITS1 + 5.8S + ITS2	GTR	6	No	0.2830
ITS1 + 5.8S + ITS2 (by eye exclusion)	GTR	6	Yes (0.2600)	0.4360
18S	TVM	6	Yes (0.7820)	0.6770
18S + ITS1 + 5.8S + ITS2	GTR	6	Yes (0.7070)	0.4850
18S + ITS1 + 5.8S + ITS2 + 5′ end 28S	GTR	6	Yes (0.6450)	0.4930

3. Results

3.1. Characteristics of ITS1 sequences and their putative secondary structures in litostomatean ciliates

The ITS1 sequences vary slightly in length from 105 nt in *Protospathidium muscicola* to 114 nt in *Monomacrocaryon terrenum*. In contrast, the GC content spans a wide range, from 17.1% in *Apobryophyllum schmidingeri* to 29.2% in *Dileptus costaricanus* (Table 5).

The litostomatean ITS1 molecules are less conserved than the ITS2 molecules, making prediction of their secondary structures less consistent. Therefore, we follow the secondary structure models of the ITS1 proposed by Ponce-Gordo et al. (2011) for *Balantidium coli* and several other litostomateans. All studied litostomatean taxa share a similar basic pattern of ITS1 secondary structure, showing an open internal loop radiating four helices (Fig. 2).

Helix I is the most consistent structural feature of the ITS1, with high base pairing conservation and low variation in length (19–21 nt). In the rhynchostomatians, helix I displays a highly conserved motif at the basal (5′-UUAA vs. UUAA-3′) and terminal (5′-CAA vs. UUG-3′) portions, which are separated by a 5′-AAC-3′ bulge situated on the 3′ side of helix I (Figs. 2 and 3). Nucleotide composition of the haptorian helix I is more variable than that of the rhynchostomatians (for comparison, see Fig. 3). Helix II is comparatively short in the rhynchostomatians (10–15 nt), presenting a very conserved motif 5′-CUU vs. GAA-3′ in the basal portion. On the other hand, helix II of the haptorians is almost two times longer (22–27 nt) and shows a relatively high variation in base pairing. Helix III is the most variable constituent of the litostomatean ITS1, with respect to its length (11–26 nt) and nucleotide composition. Helix IV is also highly variable in length (15–33 nt) and possesses a bulge in several haptorians (*Arcuospathidium* sp. and *Semispathidium* sp.) and the majority of the rhynchostomatians (*Apodileptus visscheri rhabdoplites*, *Monomacrocaryon terrenum*, *Rimaleptus mucronatus*, and *Trachelius ovum*). Helix IV has the following motif 5′-UAACU vs. GGUUG-3′ in the rhynchostomatians, while 5′-AACC(U)A(U) vs. UGGUU-3′ in the haptorians. Frequencies of bases at each position and mutual information in base-pair regions in helices I and IV are shown in the RNA structure logos (Fig. 3). The estimated thermodynamic energy of putative secondary structures of the litostomatean ITS1 is on average −10.2 kcal/mol at 37 °C.

There are zero to four GU appositions in putative secondary structure of the ITS1 transcripts (Table 5). Although these pairings are less stable than the Watson–Crick complementarities, they still retain the RNA helical structure and hence support our prediction of secondary structure.

3.2. Characteristics of ITS2 sequences and their putative secondary structures in litostomatean ciliates

The ITS2 sequences have an average length of 107 nt with a range of 105 nt (*Arcuospathidium* sp.) to 109 nt (*Cultellothrix lionotiformis*).

Table 5
Numerical and statistical values of the litostomatean ITS1 secondary structures proposed in this study.

Taxon	Length (nt)	GC content (%)	Length (nt) of each helix				Number of G–U pairing	d*G* (37 °C, kcal/mol)
			I	II	III	IV		
Apobryophyllum schmidingeri	110	17.1	20	22	11	23	0	−5.90
Apodileptus visscheri rhabdoplites	106	26.2	20	10	18	21	1	−7.30
Arcuospathidium namibiense tristicha	110	24.3	21	22	17	21	4	−14.60
Arcuospathidium sp.	112	28.3	19	25	14	24	2	−6.10
Balantidion pellucidum	111	27.0	21	23	23	15	2	−7.00
Cultellothrix lionotiformis	111	24.3	21	22	15	21	1	−10.80
Enchelyodon sp.	108	24.8	20	22	13	22	1	−10.60
Enchelys gasterosteus	113	28.9	21	24	11	20	2	−15.40
Dileptus costaricanus	112	29.2	20	12	22	24	2	−15.60
Monomacrocaryon terrenum	114	28.7	21	10	26	33	2	−10.90
Protospathidium muscicola	105	19.8	20	26	12	22	0	−4.00
Pseudomonilicaryon fraterculum	108	23.9	21	15	12	19	2	−0.80
Rimaleptus mucronatus	113	28.9	21	10	26	33	3	−12.90
Semispathidium sp.	112	24.8	20	23	20	15	1	−13.40
Spathidium sp.	112	24.8	20	27	14	22	2	−15.30
Trachelius ovum	106	21.5	20	14	16	32	0	−12.90
Trachelophyllum sp.	107	22.2	20	24	11	16	2	−9.30
Minimum	105	17.1	19	10	11	15	0	−15.6
Maximum	114	29.2	21	27	26	33	4	−0.8
Arithmetic mean	110	25.0	20.4	19.5	16.5	22.5	1.6	−10.2
Standard deviation	2.8	3.4	0.6	6.1	5.2	5.6	1.1	4.4

Table 6
Numerical and statistical values of the litostomatean ITS2 secondary structures proposed in this study.

Taxon	Length (nt)	GC content (%)	Length (nt) of each helix			Number of unpaired bases in				Number of bulges in helix III	Number of G–U pairing	dG (37 °C, kcal/mol)
			I	II	III	Interior loop	Terminal loop of helix II	Terminal loop of helix III	Bulge(s) of helix III			
Apobryophyllum schmidingeri	108	29.6	10	19	62	13	5	6	4	2	1	−24.95
Apodileptus visscheri rhabdoplites	106	37.7	10	20	44	26	4	4	4	3	4	−20.89
Arcuospathidium namibiense tristicha	107	32.7	–	21	54	32	5	6	10	3	1	−26.60
Arcuospathidium sp.	105	34.3	10	19	53	17	5	6	7	2	2	−23.45
Balantidion pellucidum	106	36.2	15	31	38	16	5	6	2	1	4	−21.42
Cultellothrix lionotiformis	109	30.3	10	19	42	22	5	4	4	2	2	−19.47
Dileptus costaricanus	106	31.1	6	20	42	19	4	4	4	3	2	−21.93
Enchelyodon sp.	106	34.9	10	19	36	28	5	6	2	1	1	−19.91
Enchelys gasterosteus	106	37.7	–	19	61	26	5	6	11	4	2	−29.10
Microdileptus microstoma	108	34.3	6	20	58	5	4	4	6	4	4	−24.70
Monomacrocaryon terrenum	108	33.3	12	20	58	14	6	4	6	4	4	−26.57
Protospathidium muscicola	107	22.4	10	19	41	14	5	4	5	2	2	−20.17
Pseudomonilicaryon fraterculum	108	32.4	17	20	46	19	4	4	6	3	3	−21.23
Rimaleptus mucronatus	108	30.6	19	20	50	15	4	4	4	3	3	−25.79
Semispathidium sp.	106	35.8	10	19	36	15	5	6	2	1	1	−26.19
Spathidium sp.	106	31.1	12	19	48	19	5	4	8	2	2	−19.93
Trachelius ovum	106	28.3	14	20	38	17	4	4	2	1	2	−26.05
Trachelophyllum sp.	106	30.2	10	21	40	26	5	6	2	1	1	−21.49
Minimum	105	22.4	6	19	36	5	4	4	2	1	1	−29.10
Maximum	109	37.7	19	31	62	32	6	6	11	4	4	−19.47
Arithmetic mean	106.8	32.4	11.3	20.3	47.1	19.1	4.7	4.9	4.9	2.3	2.3	−23.30
Standard deviation	1.1	3.7	3.5	2.8	8.8	6.6	0.6	1.0	2.7	1.1	1.1	3.0

In contrast, the GC content varies greatly from 22.4% in *Protospathidium muscicola* to 37.7% in *Enchelys gasterosteus* (Table 6).

The consensus putative secondary structure model of the ITS2 is shown in Fig. 2. Its main features include an internal loop bearing three helices of unequal length. Helix I is the shortest and most variable helix of the ITS2 molecule with a range of 6–19 nt. Helix II displays a highly conserved motif 5′-GURAGAGA vs. YCUCUYAU-3′ in its basal portion (Fig. 3) and varies in length from 19 to 21 nt. However, *Balantidion pellucidum*, as a sole exception, has an extremely elongated (31 nt) helix II which also displays a bulge near its basal portion. The terminal loop of helix II invariably comprises 5 nt (5′-AYHWU-3′) in all haptorians and 4 nt (5′-WAAV-3′) in all rhynchostomatians (except for *Monomacrocaryon terrenum*, containing 6 nt: 5′-AGACUU-3′). Helix III is longest and has one to four bulges containing on average five unpaired bases. The length of helix III spans a wide range of 36–62 nt, averaging 47 nt. In 11 out of 18 species studied, helix III presents a highly conserved motif 5′-AGCAGUCACA vs. UGUGAG-CU-3′ in its distal portion (Fig. 3). The terminal loop of helix III invariably includes 4 nt in all rhynchostomatians and in most haptorians (5′-YHHU-3′), while 6 nt in the rest of the haptorians (5′-UUHRUU-3′). The frequencies of bases at each position and mutual information in base-pair regions in helices II and III are shown in the RNA structure logos (Fig. 3). The estimated thermodynamic energy of putative secondary structures of the litostomatean ITS2 molecules spans a range of −29.10 kcal/mol to −19.47 kcal/mol at 37 °C, with an average of −23.30 kcal/mol at 37 °C.

Compensatory base changes have been revealed within the proposed putative secondary structure of the litostomatean ITS2 transcripts. Specifically, there are at most four GU appositions. One occurs invariably in the highly conserved region of helix II and zero to three are present in helix III, corroborating the proposed model.

3.3. Molecular phylogenetics and evolutionary trends of litostomatean ciliates

To determine the genealogical relationships among the litostomateans and to reconstruct their evolutionary history, we carried out 33 phylogenetic analyses based on 11 alignments using three different algorithms (Table 2). First, we performed 21 single-locus analyses on litostomatean sequences of molecules that are either involved in rRNA biogenesis (ITS1 and ITS2) or code some components for the small (18S rRNA) and large (5.8S rRNA) ribosomal subunit. Given the overall congruence between the single-locus tree topologies, though sometimes with weak support for some nodes, we compiled the following concatenated alignments: ITS1 + 5.8S + ITS2; 18S + ITS1 + 5.8S + ITS2; and 18S + ITS1 + 5.8S + ITS2 + 5′ end 28S. This second multiple-locus set of analyses resulted, as expected, in similar tree topologies as those obtained with the single-locus approach. However, most nodes were generally better supported statistically in the multiple-locus phylogenies (Table 7).

Out of 33 phylogenetic analyses performed, 31 have consistently recovered a fundamental bifurcation of the class Litostomatea into two lineages (Table 7 and Figs 4–6). The first clade is designated as subclass Rhynchostomatia. This unites free-living litostomateans having a proboscis that carries a complex oral ciliature comprising a circumoral kinety, a perioral kinety and many preoral kineties (Fig. 1A–C). The second cluster includes the free-living subclass Haptoria nesting the endocommensal subclass Trichostomatia. Members of both subclasses lack a proboscis (i.e., they have an apical oral apparatus) and have a comparatively simple oral ciliature including only a circumoral kinety and/or oralized somatic kinetids (Fig. 1 D, E, and H).

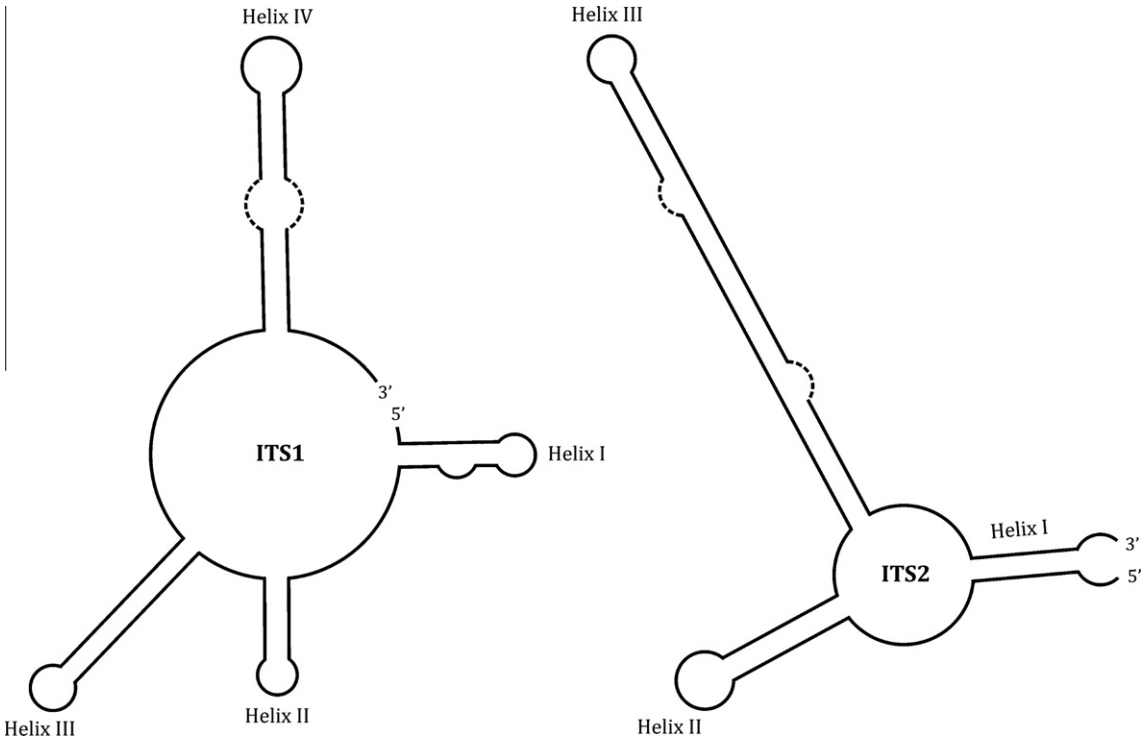

Fig. 2. Diagrams of putative secondary structure models of ITS1 and ITS2 transcripts derived by comparisons among 18 litostomatean species. Both models are supported by compensatory base changes (CBCs) that preserve the helix pairings. Dashed lines indicate bulges present in some species.

As concerns the internal relationships among the rhynchostomatians, ITS1 and ITS2 sequences considered separately were not able to unravel a well-supported branching pattern, very likely due to the mutational saturation. However, analyses of the 5.8S, 18S, and all concatenated datasets provided a well-resolved phylogeny of the rhynchostomatians. Specifically, *Trachelius ovum* represents a separate branch, the order Tracheliida, which is characterized by a curious lateral fossa, a dikinetidal circumoral kinety and an ordinary three-rowed dorsal brush. All other rhynchostomatians, i.e., the order Dileptida, are depicted as a sister group of *T. ovum* (Figs. 4–6). By contrast to the Tracheliida, the Dileptida lack a lateral fossa and are characterized by a hybrid circumoral kinety (i.e., composed of dikinetids in proboscis and monokinetids around oral opening) and a staggered two- or multi-rowed dorsal brush. The relationships at family level of the order Dileptida were not consistently recovered. The family Dimacrocaryonidae (represented here by *Microdileptus microstoma*, *Monomacrocaryon terrenum* and *Rimaleptus mucronatus*; however, *M. microstoma* was included only in the 5.8S, ITS2, and 18S datasets, as we were not able to obtain its full ITS1 sequence), which typically has one or two macronuclear nodules and a single micronucleus, was found as monophyletic in 21 out of 33 analyses (Table 7). The family Dileptidae (represented here by *Apodileptus visscheri rhabdoplites*, *Dileptus costaricanus* and *Pseudomonilicaryon fraterculum*), which is defined by having at least four macronuclear nodules and many micronuclei, was depicted as monophyletic only in the 5.8S, 18S, and 18S + ITS1 + 5.8S + ITS2 analyses (Table 7 and Fig. 5). In the other analyses, *P. fraterculum* did not group with *D. costaricanus* and *A. visscheri rhabdoplites*, but was placed basally within the order Dileptida, however, with low support (Figs. 4 and 6). Nevertheless, the monophyly of the family Dileptidae could not be rejected by the approximately unbiased (*P*-value = 0.480) and the Shimodaira–Hasegawa (*P*-value = 0.475) statistical topology tests carried out on the largest 18S + ITS1 + 5.8S + ITS2 + 5′ end 28S dataset.

The internal relationships within the Haptoria–Trichostomatia clade were not well resolved in any dataset, suggesting one or several radiation event(s) and/or undersampling of haptorian and trichostomatian genera. However, we have identified several common branching patterns (Table 7 and Figs. 4–6). (1) The orders Spathidiida and Haptorida always grouped together. (2) Two spathidiids, *Apobryophyllum schimidingeri* and *Cultellothrix lionotiformis*, consistently formed a strongly supported monophylum. These two species, in contrast to all other spathidiids included in the analyses, display a dorsal brush on the left (vs. dorsal) side of the body. (3) Two traditional haptorids, *Balantidion pellucidum* and *Enchelys gasterosteus*, consistently clustered together with strong support. Unlike all haptorians in the dataset, they share oralized somatic monokinetids. (4) The subclass Trichostomatia was monophyletic and usually branched within the order Spathidiida or was placed in the basal polytomy of the free-living haptorians. The approximately unbiased (*P*-value = 0.348) and Shimodaira–Hasegawa (*P*-value = 0.276) topology tests were not able to significantly reject the sister relationship of the Trichostomatia and Haptoria for the 18S + ITS1 + 5.8S + ITS2 dataset. However, this could be caused by the strong undersampling of trichostomatian sequences in the dataset.

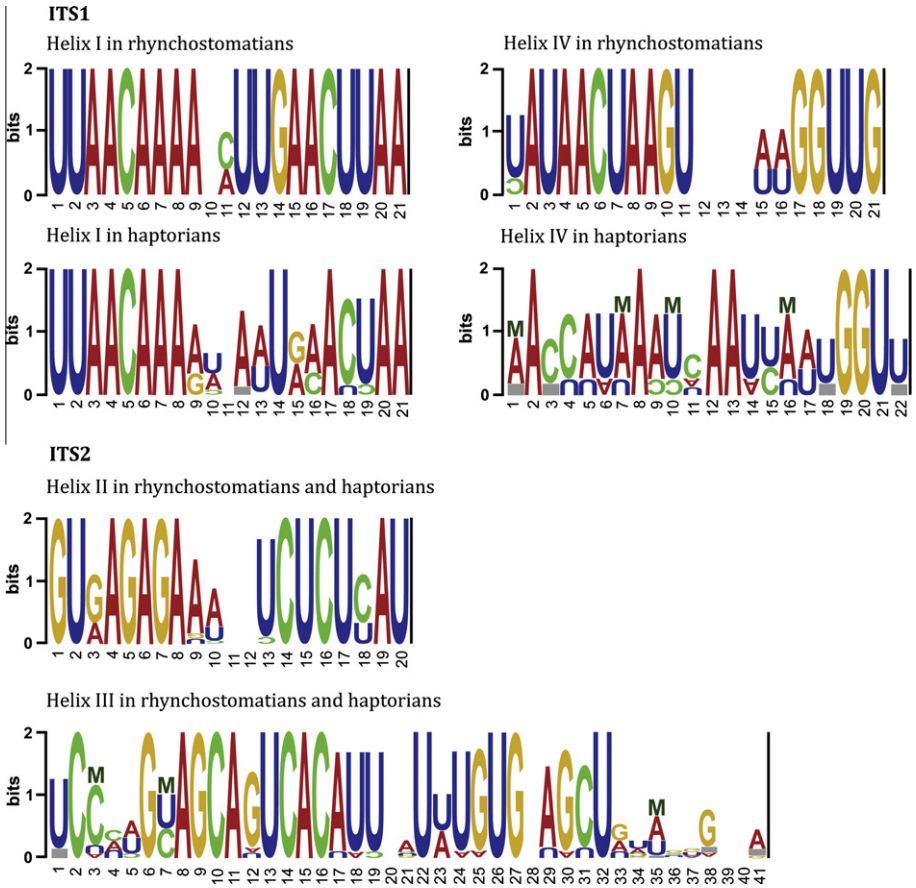

Fig. 3. ITS structure logo of litostomateans. The height of a base in each column is proportional to its frequency in multiple sequence alignments. The relative entropy method was used where the frequency of bases in each column is compared to the background frequency of each base. A prior nucleotide distribution was set to A:C:G:U = 1:1:1:1. Inverted sequence characters indicate a less-than-background frequency. Mutual information in pairs of columns is indicated by the letter M.

4. Discussion

4.1. Primary sequence and structural evolution of ITS1

The internal transcribed spacer 1 (ITS1) lies between the regions coding for 18S rRNA and 5.8S rRNA gene (Maroteaux et al., 1985). Some structural elements of the ITS1 could play a role in the cleavage of the pre-18S rRNA molecule at the ITS1 site (van Nues et al., 1994). This process is controlled to some extent by the interaction of the 18S rRNA precursor with some small nucleolar RNAs, indicating a minor function of the ITS1 in the rRNA processing. This, in turn, permits large variations both in the primary sequence and in the secondary structure of the ITS1 gene between various groups of organisms (Ferreira-Cerca, 2008; Ponce-Gordo et al., 2011).

In general, the putative secondary structure of the ITS1 transcripts includes an open loop with a different number of helices, ranging from three in peritrich ciliates (Sun et al., 2010) to seven in flatworms (von der Schulenburg et al., 1999), and up to nine in plants (Kan et al., 2007). In the free-living litostomatean ciliates, our results and those of Ponce-Gordo et al. (2011) indicate that there are four helices radiating from a 5′–3′ common loop, matching the ciliate ITS1 secondary structure models proposed by Hoshina (2010) and Sun et al. (2010). However, in the endocommensal litostomateans, there is an extra helix E1 which separates helix I from the other three helices (Ponce-Gordo et al., 2011). This different pattern was explained by the minor role of the ITS1 in the rRNA processing, enabling large variations also in the secondary structure (see above). On the other hand, helix I is the most conserved feature in the secondary structure of the litostomatean ITS1 transcript, with respect to its length and nucleotide composition (Ponce-Gordo et al., 2011; Table 5 and Fig. 3). This suggests that helix I could play an important role in the pre-18S rRNA molecule cleavage at the 5′ site of the ITS1.

4.2. Primary sequence and structural evolution of ITS2

The internal transcribed spacer 2 (ITS2) lies between the 5.8S and 28S rRNA region and is important in the maturation processes of both the 5.8S and 28S rRNA molecules (Ferreira-Cerca, 2008; Maroteaux et al., 1985). This causes the primary and secondary structure of the ITS2 transcript to be rather conserved in eukaryotes (Coleman, 2003; Schultz et al., 2005; Wolf et al., 2005). In ciliates, two models were recognized: a "ring model" with a common loop radiating three to four helices (Coleman, 2005; Miao et al., 2008; Ponce-Gordo et al., 2011) and a "hairpin model" in which the common loop is started and closed by helix I and bears only helices II and III; helix IV, if present, is located between helix I and the 28S rRNA region (Sun et al., 2010). Côté et al. (2002) proposed a dynamic conformational model for the role of ITS2 processing: initial formation of the ring structure may be required for essential, early events in processing complex assembly and

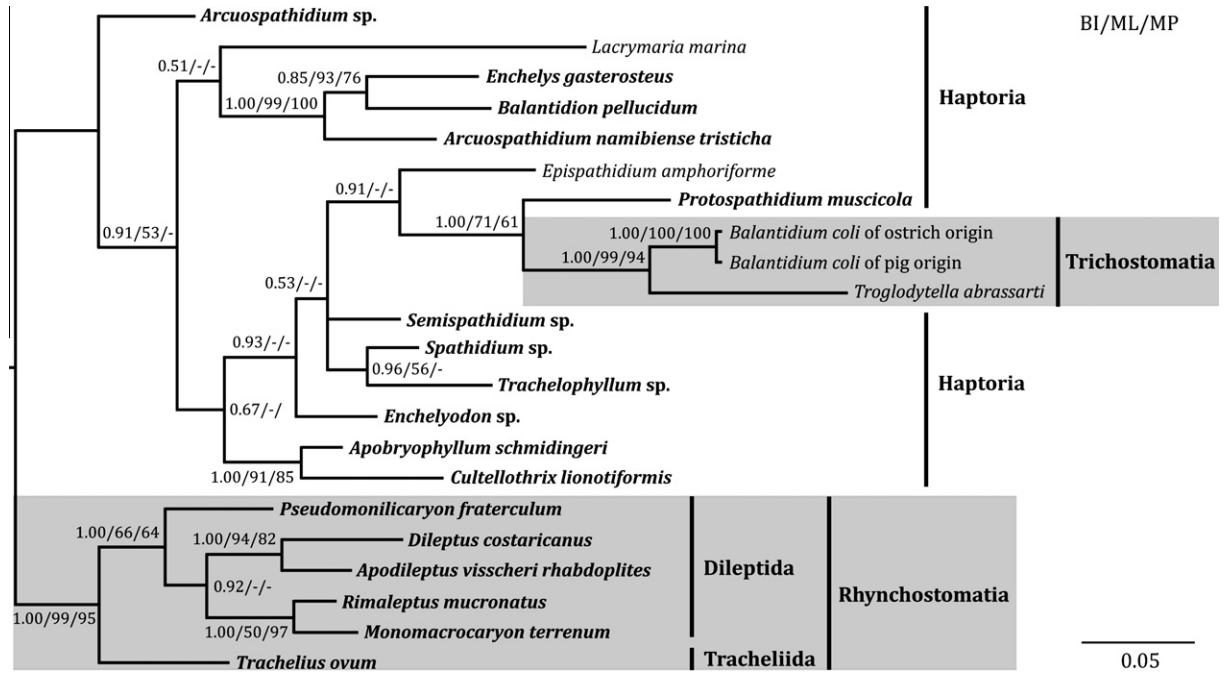

Fig. 4. Concatenated ITS1 + 5.8S + ITS2 phylogeny based on 341 unambiguously aligned nucleotide characters of 22 taxa from the class Litostomatea. Three methods (Bayesian inference, maximum likelihood, and maximum parsimony) were used for tree construction. Posterior probabilities for the Bayesian inference (BI) and bootstrap values for maximum likelihood (ML) and maximum parsimony (MP) analyses are shown at nodes (a dash indicates bootstrap values below 50%). Sequences in bold were obtained during this study. The scale bar indicates the fraction of substitutions per site.

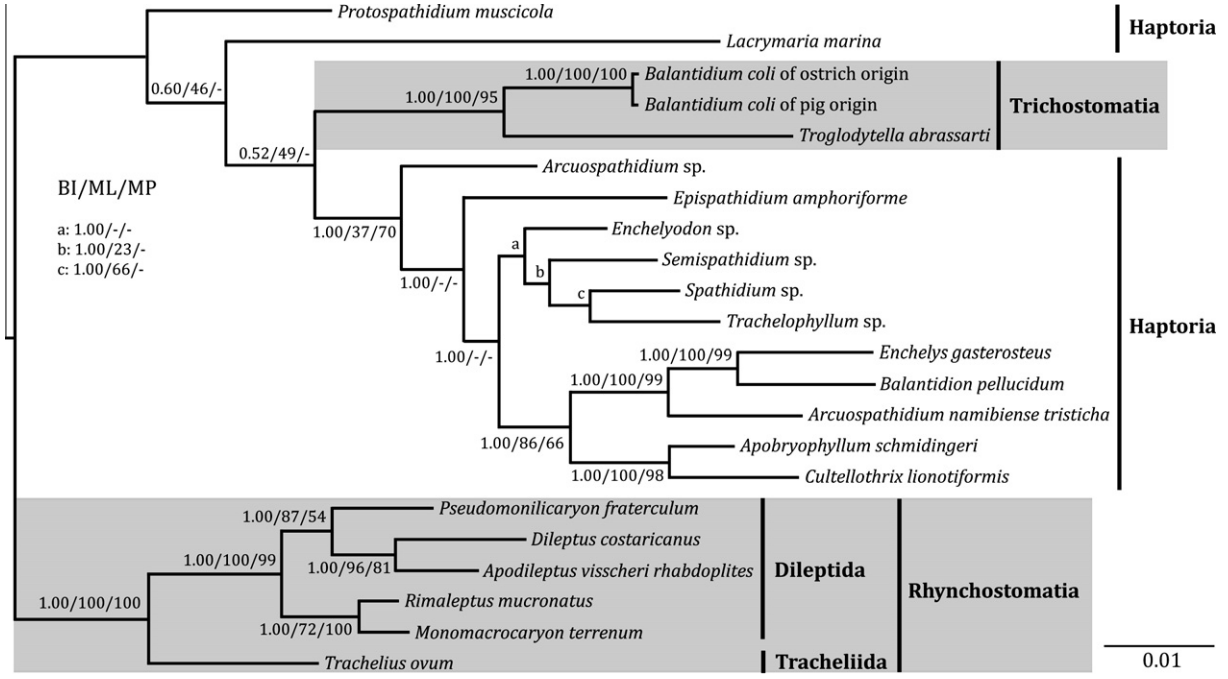

Fig. 5. Concatenated 18S + ITS1 + 5.8S + ITS2 phylogeny based on 1832 unambiguously aligned nucleotide characters of 22 taxa from the class Litostomatea. Three methods (Bayesian inference, maximum likelihood, and maximum parsimony) were used for tree construction. Posterior probabilities for the Bayesian inference (BI) and bootstrap values for maximum likelihood (ML) and maximum parsimony (MP) analyses are shown at nodes (a dash indicates bootstrap values below 50%). The scale bar indicates the fraction of substitutions per site.

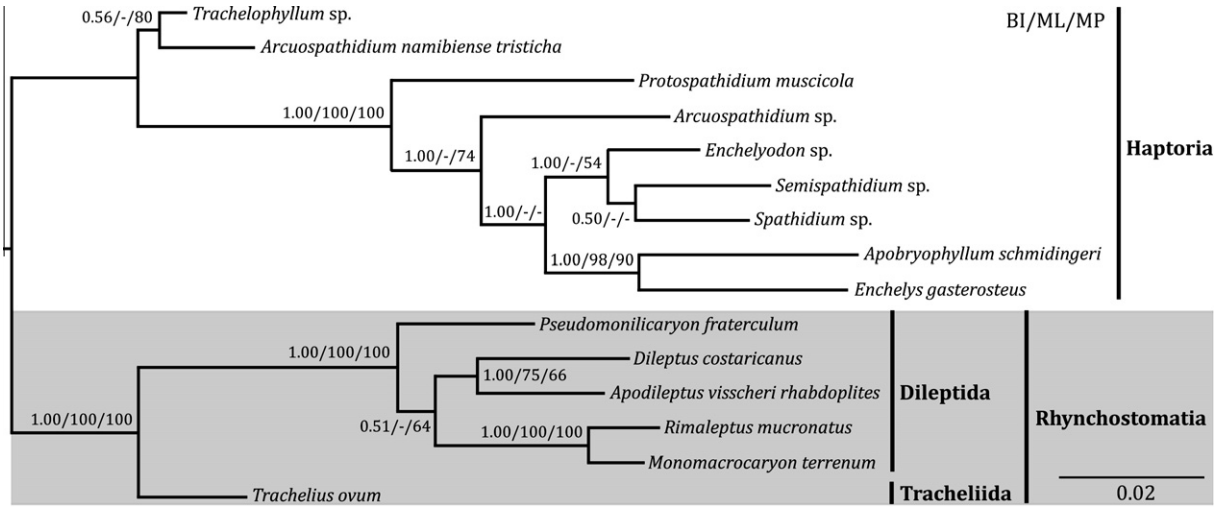

Fig. 6. Concatenated 18S + ITS1 + 5.8S + ITS2 + 5′ end 28S phylogeny based on 2310 unambiguously aligned nucleotide characters of 15 taxa from the class Litostomatea. Three methods (Bayesian inference, maximum likelihood, and maximum parsimony) were used for tree construction. Posterior probabilities for the Bayesian inference (BI) and bootstrap values for maximum likelihood (ML) and maximum parsimony (MP) analyses are shown at nodes (a dash indicates bootstrap values below 50%). The scale bar indicates the fraction of substitutions per site.

Table 7
Comparison of statistical support in chosen nodes.

Alignment	No. of characters	Phylogenetic method	Nodal support							
			A	B	C	D	E	F	G	H
5.8S	150	BI	0.83	0.77	0.82	–	–	0.83	0.99	–
		ML	78	38	78	26	–	78	63	–
		MP	67	–	–	60	–	67	55	–
5.8S (by eye exclusion)	144	BI	0.97	0.56	0.68	–	–	0.97	0.50	–
		ML	74	28	60	–	–	74	–	–
		MP	73	–	–	–	–	73	–	–
ITS1	135	BI	1.00	–	–	1.00	0.86	1.00	0.52	66
		ML	94	–	–	99	–	94	63	65
		MP	88	–	–	100	–	88	–	–
ITS1 (by eye exclusion)	98	BI	1.00	–	–	1.00	0.90	1.00	0.67	0.68
		ML	87	–	–	96	–	87	61	69
		MP	61	–	–	85	89	61	–	58
ITS2	114	BI	0.89	–	–	0.59	0.70	0.89	0.96	0.98
		ML	59	–	–	32	–	59	–	81
		MP	53	–	–	–	–	53	68	66
ITS2 (by eye exclusion)	99	BI	0.94	–	–	0.51	0.78	0.94	0.69	0.65
		ML	–	–	–	34	–	–	–	69
		MP	–	–	–	–	58	–	52	–
ITS1 + 5.8S + ITS2	399	BI	1.00	1.00	–	1.00	1.00	1.00	1.00	1.00
		ML	100	63	–	100	48	100	97	98
		MP	94	–	–	96	92	94	86	91
ITS1 + 5.8S + ITS2 (by eye exclusion)	341	BI	1.00	1.00	–	1.00	1.00	1.00	1.00	0.85
		ML	99	66	–	94	50	99	91	93
		MP	95	64	–	82	97	95	85	76
18S	1493	BI	1.00	1.00	–	–	1.00	1.00	1.00	1.00
		ML	100	100	41	–	100	100	98	85
		MP	100	100	–	–	89	100	99	76
18S + ITS1 + 5.8S + ITS2	1832	BI	1.00	1.00	1.00	1.00	1.00	1.00	1.00	1.00
		ML	100	100	87	96	72	100	100	100
		MP	100	99	54	81	100	100	98	99
18S + ITS1 + 5.8S + ITS2 + 5′ end 28S	2310	BI	1.00	1.00	–	1.00	1.00	1.00	?	?
		ML	100	100	49	75	100	100	?	?
		MP	100	100	–	66	100	100	?	?

Dash (–) indicates that node was not recovered with support >0.50 for BI, >20 for ML, and >50 for MP analyses. Question mark (?) indicates relationships untested due to unavailable sequence data.

A – monophyly of the subclass Rhynchostomatia; B – monophyly of the order Dileptida; C – monophyly of the family Dileptidae; D – monophyly of dileptids with many scattered macronuclear nodules, i.e., *Apodileptus visscheri rhabdoplites* and *Dileptus costaricanus*; E – monophyly of the family Dimacrocaryonidae, i.e., *Microdileptus microstoma*, *Monomacrocaryon terrenum*, and *Rimaleptus mucronatus* (however, *M. microstoma* was included only in the 5.8S, ITS2, and 18S datasets, as we were not able to obtain its full ITS1 sequence); F – monophyly of the subclasses Haptoria and Trichostomatia; G – monophyly of spathidiids with laterally located dorsal brush, i.e., of *Apobryophyllum schmidingeri* and *Cultellothrix lionotiformis*; H – monophyly of traditional haptorids with oralized somatic monokinetids, i.e., of *Balantidion pellucidum* and *Enchelys gasterosteus*.

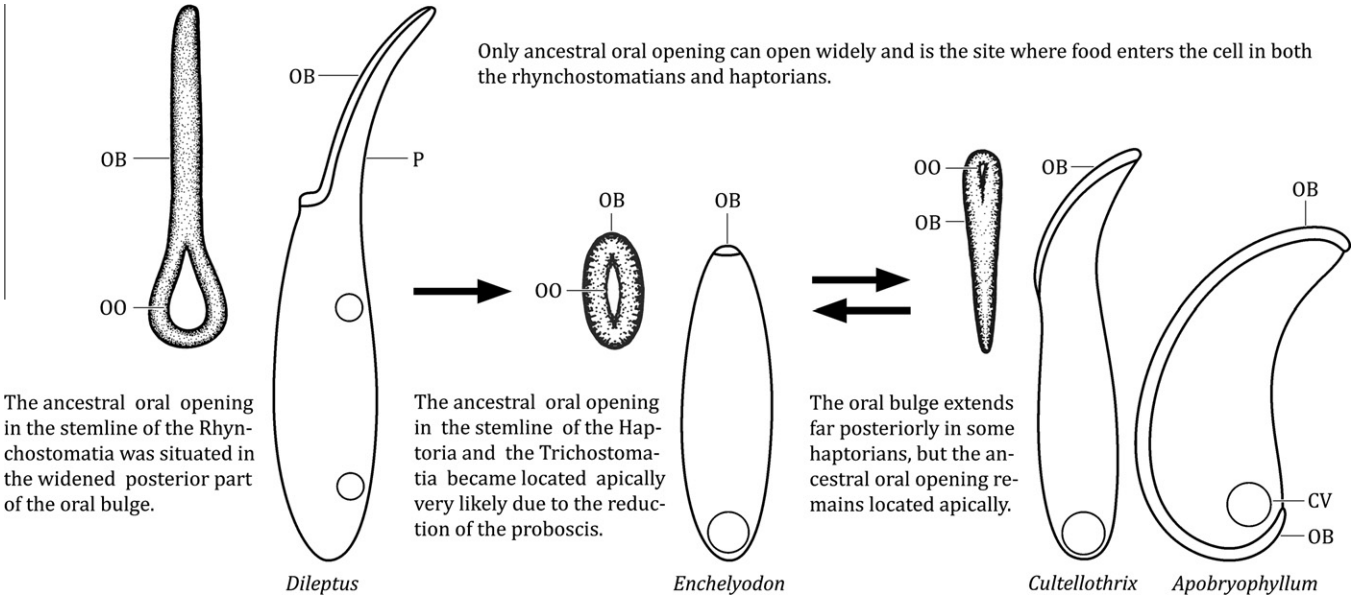

Fig. 7. Hypothesis for the evolution of the haptorian polar body organization from a *Dileptus*-like progenitor with a ventrally positioned oral opening. CV, contractile vacuole; OB, oral bulge; OO, oral opening; P, proboscis.

followed by an induced transition to the hairpin strucuture that facilitates subsequent processing events. This dynamic model explains very well the existence of both the hairpin model predicted for our litostomatean ITS2 transcripts, and the ring model proposed for the litostomatean ITS sequences by Ponce-Gordo et al. (2011). Both litostostomatean ITS2 models match very well in the structure and motifs of helices II and III, but differ in helix I which is very likely the dynamic constituent of the ITS2 transcripts, enabling switching from the ring to the hairpin pattern.

The litostomatean ITS2 molecules differ from those of oligohymenophorean ciliates by lack of the pyrimidine–pyrimidine bulge in helix II (Coleman, 2005; Miao et al., 2008; Sun et al., 2010), as already recognized by Ponce-Gordo et al. (2011). Spirotrichean ciliates also lack the pyrimidine–pyrimidine bulge in helix II which is designated as helix A (Gao et al., 2010; Weisse et al., 2008; Yi et al., 2008). This supports the 18S rRNA gene megaclassification of intramacronucleate ciliates in that litostomateans, armophoreans and spirotricheans form a super-clade which is sister to ventrate ciliates including oligohymenophoreans (Cavalier-Smith, 2004; Vd'ačný et al., 2010). On the other hand, spirotrichean helix III, which is designated as helix B, consistently displays a multibranch pattern not occurring in litostomateans (Gao et al., 2010; Ponce-Gordo et al., 2011; Weisse et al., 2008; Yi et al., 2008; present study). Thus, the secondary structures of the ITS2 molecules may help to unravel the deep evolutionary history of intramacronucleate ciliates, whose relationships are still poorly understood.

4.3. ITS sequences as a tool for reconstructing deep evolutionary history

The ITS region is frequently utilized for phylogenetic analyses at the genus and species levels in ciliates (e.g., Ponce-Gordo et al., 2011; Stoeck et al., 2007; Weisse et al., 2008; Yi et al., 2008). However, application of the ITS region in unraveling phylogeny at higher taxonomic levels was previously limited by uncertainties in alignment due to excessive insertions, deletions and mutational saturations. Coleman (2003) argued that the secondary structure of the ITS transcripts provides the key to solve this problem. Indeed, the present and previous studies (Coleman, 2005; Miao et al., 2008; Sun et al., 2010) on various ciliate groups document that ITS molecules have an appropriate signal for untangling relationships not only at species level but also at higher taxonomic ranks, when their secondary structure information is utilized to aid alignment. Thus, once secondary structure has been established for the litostomatean ITS transcripts, their sequences can be aligned across broader taxonomic levels including subclasses and orders. With multiple loci of a few hundred nucleotides, one can analyze relationships among the litostomateans from the subspecies to the subclass rank.

It is important to note that insertions and deletions within of the ITS sequences seem to be also an important phylogenetic marker, resulting in various sequence lengths. Specifically, spirotricheans possess the longest ITS transcripts, while litostomateans display the shortest ones, having 35–100 nt fewer than other ciliates (Coleman, 2005; Hoshina, 2010; Miao et al., 2008; Ponce-Gordo et al., 2011; Stoeck et al., 2007; Sun et al., 2010; Weisse et al., 2008; Yi et al., 2008; present study). Similarly, the litostomatean 18S rRNA gene is shorter in comparison with other ciliates due to the deletions in helices 23–1, 23–8, 23–9, and the absence of the entire helix 23–5 (Leipe et al., 1994; Strüder-Kypke et al., 2006; Vd'ačný et al., 2011a,b; Wright and Lynn, 1997a,b; Wright et al., 1997). The comparatively short 18S rRNA, ITS1 and ITS2 sequences in all litostomatean ciliates indicate that one or several deletion events occurred in the rRNA gene region of their last common ancestor.

4.4. ITS sequences as a tool for testing the reliability of 18S rRNA gene phylogenies

To test whether 18S rRNA gene provides a suitable proxy for reconstruction of the litostomatean evolutionary history, we used the ITS region sequences. Although these are localized on the same transcriptional unit as 18S and 28S rRNA genes, only 5.8S rRNA molecule is incorporated into the ribosome, while ITS1 and ITS2 are removed from the transcript and consequently degraded (e.g., Retèl and Planta, 1967). This very likely causes that ITS sequences are subject to reasonably mild functional constraints which, in turn, enables a comparatively frequent occurrence of insertions and deletions as well as a preponderance of nucleotide sites that would evolve essentially neutrally (Álvarez and Wendel, 2003). Thus, in relation to functionality, it can be assumed that ITS sequences are not the same "unit of selection" as rRNA genes. Consequently, ITS1 and ITS2 could be used as a rather independent test

whether 18S rRNA molecules elucidate the litostomatean phylogeny properly. Because ITS1 and ITS2 phylogenies are congruent with 18S rRNA gene trees, we find 18S rRNA molecules as an effective tool for unraveling the litostomatean evolutionary history. This is also supported by the highest values of tree indices for the 18S rRNA gene dataset, i.e., consistency index (CI), consistency index excluding uninformative characters (CIex), retention index (RI), and rescaled consistency index (RC) show the best fit of the 18S rRNA data to the inferred phylogenetic trees (Table 2).

4.5. Molecular and morphological evolution of litostomatean ciliates

The monophyletic origin of the class Litostomatea was consistently supported by five strong morphological apomorphies and the 18S rRNA gene (for review, see Vd'ačný et al., 2011a). However, the morphology-based phylogenetic relationships among the litostomateans conflict with the 18S rRNA gene phylogenies, especially, in that (1) the Litostomatea are not subdivided into the free-living haptorians (including also rhynchostomatians) and the endocommensal trichostomatians (Foissner and Foissner, 1988; Jankowski, 2007; Lynn, 2008; Lynn and Small, 2002), but into the free-living rhynchostomatians and the free-living haptorians including the endocommensal trichostomatians (Vd'ačný et al., 2011a,b); (2) rhynchostomatians, the crown litostomateans with the most complex morphology and ontogenesis, do not represent highly derived spathidiids (Vd'ačný and Foissner, 2008, 2009; Xu and Foissner, 2005), but are classified at the base of the Litostomatea as a sister group of all other litostomateans (Vd'ačný et al., 2011a,b); (3) simple polar enchelyine haptorids without circumoral kinety have not been found as an ancestral group of the litostomateans, but rather are nested within the spathidiid cluster (Foissner, 1984; Foissner and Foissner, 1985; Vd'ačný et al., 2011a); (4) spathidiids and haptorids have been not recovered as separate monophyla, but are mixed together usually without any clear morphological connection (Foissner and Foissner, 1988; Jankowski, 2007; Lynn, 2008; Vd'ačný et al., 2011a); and (5) the endocommensal trichostomatians are shown originating from rapacious terrestrial spathidiids, such as *Epispathidium papilliferum* or *Protospathidium muscicola* (Foissner and Foissner, 1985; Gao et al., 2008; Pan et al., 2010; Strüder-Kypke et al., 2006, 2007; Vd'ačný et al., 2010, 2011a,b). In our previous studies, we were able to overcome most of these conflicting issues by suggesting body polarization and simplification of the oral apparatus as the main evolutionary trends in the Litostomatea (for details, see Vd'ačný et al., 2010, 2011a,b and below). Indeed, our proposed reconstruction of the deep litostomatean evolutionary history is in a good agreement with single-locus trees inferred from 5.8S rRNA, ITS1, and ITS2 as well as with multiple-locus trees inferred from the whole ITS region and its concatenation with the 18S rRNA gene and the first two domains of the 28S rRNA gene.

4.6. Body apicalization in litostomatean evolution

Body polarization, i.e., apicalization of the oral opening, has been revealed as one of the main evolutionary trends in the litostomateans (see above). Most intramacronucleate ciliates including armophoreans, the supposed sister group of the litostomateans, have a ventral oral opening and a complex oral ciliature (Cavalier-Smith, 2004; Jankowski, 2007; Lynn, 2008; Vd'ačný et al., 2010). Within the Litostomatea, only rhynchostomatians display this plesiomorphic body organization (Vd'ačný et al., 2010, 2011a,b). Therefore, Vd'ačný et al. (2011a) used the morphology of the rhynchostomatians and armophoreans to hypothesize that the last common ancestor of the Litostomatea had a keyhole-shaped oral bulge with the oral opening situated in the widened posterior part (Fig. 1A and B). This is the only site of the rhynchostomatian oral bulge that can open and ingest prey (Dragesco, 1962; Vd'ačný and Foissner, 2012; Visscher, 1923; Fig. 1C). In contrast, the oral opening of the stemline of the Haptoria and Trichostomatia was very likely located apically and in the centre of the oral bulge (Vd'ačný et al., 2011a; Fig. 1D and E). This pattern possibly evolved by reduction of the proboscis causing only the posterior portion of the oral bulge, which surrounds the ancestral oral opening, to remain and become located in the anterior body pole (Fig. 7). Even when the oral bulge extends far posteriorly (e.g., in bryophyllids and pleurostomatids), only its apical portion opens during feeding like in simple polar haptorians (Dragesco, 1962; Foissner and Lei, 2004; Foissner and Xu, 2007; Foissner et al., 1995, 1999, 2002; Guhl and Hausmann, 2008; Maupas, 1883; Woodruff and Spencer, 1921, 1922; Fig. 1G, I, and J). As concerns the trichostomatians, the polar position of the oral opening was maintained in the archistomatids, such as *Wolskana*, *Didesmis*, and *Alloiozona*, while in more derived vestibuliferids and isotrichids the opening sunk into an anterior vestibulum or was displaced posteriorly (Grain, 1966; Lynn, 2008; Lynn and Small, 2002; Vd'ačný et al., 2011a). To summarize, the oral opening is located far subapically in the rhynchostomatians, while apically in all haptorians and basal trichostomatians. We find this differing location of the oral opening as the key morphological trait, explaining the deep split of the Litostomatea into Rhynchostomatia and Haptoria + Trichostomatia.

5. Conclusions

The following conclusions can be drawn from the present phylogenetic analyses:

(1) The 18S rRNA gene is an effective tool for unraveling the litostomatean phylogeny because three additional markers (ITS1, 5.8S rRNA, and ITS2) indicate the same or very similar phylogenetic relationships for the Litostomatea.
(2) ITS1 and ITS2 sequences can be used to infer phylogenetic relationships among litostomateans not only at the species level but also at higher taxonomic ranks, when their secondary structure information is utilized to aid alignment.
(3) The comparatively short 18S rRNA, ITS1 and ITS2 sequences in all litostomatean ciliates indicate that one or several deletion events occurred in the rRNA gene region of their last common ancestor.
(4) According to both single-locus and multiple-locus phylogenetic analyses, there are two distinct litostomatean lineages: Rhynchostomatia and Haptoria + Trichostomatia.
(5) Body polarization and simplification of the oral apparatus are the main evolutionary trends in the Litostomatea. The location of the oral opening is the most important morphological phylogenetic marker, explaining the deep split of the Litostomatea into Rhynchostomatia and Haptoria + Trichostomatia.

Acknowledgments

Financial support was provided by the Austrian Science Foundation (FWF Projects P-19699-B17 and P-20360-B17 to Wilhelm Foissner), the Slovak Scientific Grant Agency (VEGA Project 1/0600/11 to Peter Vd'ačný), and US NSF Grants (Projects MCB-0348341 and DEB-0816840 to Slava S. Epstein). The technical assistance of Mgr. Marek Vd'ačný, Mag. Gudrun Fuß, Mag. Barbara Harl and Robert Schörghofer is greatly appreciated.

References

Álvarez, I., Wendel, J.F., 2003. Ribosomal ITS sequences and plant phylogenetic inference. Mol. Phylogenet. Evol. 29, 417–434.

Bernhart, S.H., Hofacker, I.L., Will, S., Gruber, A.R., Stadler, P.F., 2008. RNAalifold: improved consensus structure prediction for RNA alignments. BMC Bioinform. 9, 474.

Cavalier-Smith, T., 2004. Chromalveolate diversity and cell megaevolution: interplay of membranes, genomes and cytoskeleton. In: Hirt, R.P., Horner, D.S. (Eds.), Organelles, Genomes and Eukaryote Phylogeny. CRC Press, Boca Raton, London, New York, Washington, DC, pp. 75–108.

Coleman, A.W., 2003. ITS2 is a double-edged tool for eukaryote evolutionary comparisons. Trends Genet. 19, 370–375.

Coleman, A.W., 2005. *Paramecium aurelia* revisited. J. Eukaryot. Microbiol. 52, 68–77.

Côté, C.A., Greer, C.L., Peculis, B.A., 2002. Dynamic conformational model for the role of ITS2 in pre-rRNA processing in yeast. RNA 8, 786–797.

Dragesco, J., 1962. Capture et ingestion des proies chez les infusoires ciliés. Bull. Biol. Fr. Belg. 96, 123–167.

Ferreira-Cerca, S., 2008. Analysis of the In Vivo Functions and Assembly Pathway of Small Subunit Ribosomal Proteins in *Saccharomyces cerevisiae*. PhD Thesis, Universität Regensburg. <http://epub.uniregensburg.de/10718/1/FerreiraCercaS.pdf>.

Foissner, W., 1984. Infraciliatur, Silberliniensystem und Biometrie einiger neuer und wenig bekannter terrestrischer, limnischer und mariner Ciliaten (Protozoa: Ciliophora) aus den Klassen Kinetofragminophora, Colpodea und Polyhymenophora. Stapfia 12, 1–165.

Foissner, W., 1991. Basic light and scanning electron microscopic methods for taxonomic studies of ciliated protozoa. Eur. J. Protistol. 27, 313–330.

Foissner, W., Foissner, I., 1985. Oral monokinetids in the free-living haptorid ciliate *Enchelydium polynucleatum* (Ciliophora, Enchelyidae): ultrastructural evidence and phylogenetic implications. J. Protozool. 32, 712–722.

Foissner, W., Foissner, I., 1988. The fine structure of *Fuscheria terricola* Berger et al., 1983 and a proposed new classification of the subclass Haptoria Corliss, 1974 (Ciliophora, Litostomatea). Arch. Protistenk. 135, 213–235.

Foissner, W., Lei, Y.-L., 2004. Morphology and ontogenesis of some soil spathidiids (Ciliophora, Haptoria). Linzer Biol. Beitr. 36, 159–199.

Foissner, W., Xu, K., 2007. Monograph of the Spathidiida (Ciliophora, Haptoria): Protospathidiidae, Arcuospathidiidae, Apertospathulidae, vol. I. Springer Verlag, Dordrecht.

Foissner, W., Berger, H., Blatterer, H., Kohmann, F., 1995. Taxonomische und ökologische Revision der Ciliaten des Saprobiensystems – Band IV: Gymnostomatea, *Loxodes*, Suctoria. Informationsberichte des Bayer. Landesamtes für Wasserwirtschaft 1 (95), 1–540.

Foissner, W., Berger, H., Schaumburg, J., 1999. Identification and ecology of limnetic plankton ciliates. Informationsberichte des Bayer. Landesamtes für Wasserwirtschaft 3 (99), 1–793.

Foissner, W., Agatha, S., Berger, H., 2002. Soil ciliates (Protozoa, Ciliophora) from Namibia (Southwest Africa) with emphasis on two contrasting environments, the Etosha region and the Namib Desert. Denisia 5, 1–1459.

Gao, F., Yi, Z., Gong, J., Al-Rasheid, K.A.S., Song, W., 2010. Molecular phylogeny and species separation of five morphologically similar *Holosticha*-complex ciliates (Protozoa, Ciliophora) using ARDRA ribroprinting and multigene sequence data. Chin. J. Oceanol. Limnol. 28, 542–548.

Gao, S., Song, W., Ma, H., Clamp, J.C., Yi, Z., Al-Rasheid, K.A.S., Chen, Z., Lin, X., 2008. Phylogeny of six genera of the subclass Haptoria (Ciliophora, Litostomatea) inferred from sequences of the gene coding for small subunit ribosomal RNA. J. Eukaryot. Microbiol. 55, 562–566.

Gorodkin, J., Heyer, L.J., Brunak, S., Stormo, G.D., 1997. Displaying the information contents of structural RNA alignments: the structure logos. Comput. Appl. Biosci. 13, 583–586.

Grain, J., 1966. Étude cytologique de quelques ciliés holotriches endocommensaux des ruminants et des équidés. Protistologica 2, 5–51, 59–141.

Grain, J., 1994. Classe de Litostomatea. In: Puytorac, P. de (Ed.), Infusoires Ciliés–Systematique. Traité de Zoologie. Fasc. 2, vol. 2. Masson, Paris, pp. 267–310.

Griffiths-Jones, S., Moxon, S., Marshall, M., Khanna, A., Eddy, S.R., Bateman, A., 2005. Rfam: annotating non-coding RNAs in complete genomes. Nucl. Acids Res. 33, 121–124.

Gruber, A.R., Lorenz, R., Bernhart, S.H., Neuböck, R., Hofacker, I.L., 2008. The Vienna RNA Websuite. Nucl. Acids Res. 36 (Suppl. 2), W70–W74.

Guhl, A., Hausmann, K., 2008. Nahrungserwerb und Nahrungsaufnahme beim Ciliaten *Didinium nasutum* – rasterelektronenmikroskopische Ergänzungen. Denisia 23, 371–381.

Hall, T.A., 1999. BioEdit: a user-friendly biological sequence alignment editor and analysis program for Windows 95/98/NT. Nucl. Acids Symp. Ser. 41, 95–98.

Hoshina, R., 2010. Secondary structural analyses of ITS1 in *Paramecium*. Microbiol. Environ. 25, 313–316.

ICZN (International Commission on Zoological Nomenclature), 1999. International Code of Zoological Nomenclature, fourth ed. Tipografia La Garangola, Padova.

Jankowski, A.W., 2007. Tip Ciliophora Doflein, 1901 [Phylum Ciliophora Doflein, 1901]. In: Alimov, A.F. (Ed.), Protisty: Rukovodstvo po zoologii, č. 2 [Protista: Handbook of Zoology, 2nd part]. Nauka, St. Petersburg, pp. 415–993 (in Russian with English title translation).

Jerome, C.A., Lynn, D.H., 1996. Identifying and distinguishing sibling species in the *Tetrahymena pyriformis* complex (Ciliophora, Oligohymenophorea) using PCR/RFLP analysis of nuclear ribosomal DNA. J. Eukaryot. Microbiol. 43, 492–497.

Kan, X.Z., Wang, S.S., Ding, X., Wang, X.Q., 2007. Structural evolution of rDNA ITS in Pinaceae and its phylogenetic implications. Mol. Phylogenet. Evol. 44, 765–777.

Keller, A., Schleicher, T., Schultz, J., Müller, T., Dandekar, T., Wolf, M., 2009. 5.8S-28S rRNA interaction and HMM-based ITS2 annotation. Gene 430, 50–57.

Koetschan, C., Förster, F., Keller, A., Schleicher, T., Ruderisch, B., Schwarz, R., Müller, T., Wolf, M., Schultz, J., 2010. The ITS2 database III – sequences and structures for phylogeny. Nucl. Acids Res. 38 (Suppl. 1), D275–D279.

Larkin, M.A., Blackshields, G., Brown, N.P., Chenna, R., McGettigan, P.A., McWilliam, H., Valentin, F., Wallace, I.M., Wilm, A., Lopez, R., Thompson, J.D., Gibson, T.J., Higgins, D.G., 2007. Clustal W and Clustal X version 2.0. Bioinformatics 23, 2947–2948.

Leipe, D.D., Bernhard, D., Schlegel, M., Sogin, M.L., 1994. Evolution of 16S-like ribosomal RNA genes in the ciliophoran taxa Litostomatea and Phyllopharyngea. Eur. J. Protistol. 30, 354–361.

Ludwig, W., Strunk, O., Westram, R., Richter, L., Meier, H., Yadhukumar, Buchner, A., Lai, T., Steppi, S., Jobb, G., Förster, W., Brettske, I., Gerber, S., Ginhart, A.W., Gross, O., Grumann, S., Hermann, S., Jost, R., König, A., Liss, T., Lüßmann, R., May, M., Nonhoff, B., Reichel, B., Strehlow, R., Stamatakis, A., Stuckmann, N., Vilbig, A., Lenke, M., Ludwig, T., Bode, A., Schleifer K.-H., 2004. ARB: a software environment for sequence data. Nucl. Acids Res. 32, 1363–1371.

Lynn, D.H., 2008. The Ciliated Protozoa. Characterization, Classification, and Guide to the Literature, third ed. Springer, Dordrecht.

Lynn, D.H., Small, E.B., 2002. Phylum Ciliophora. In: Lee, J.J., Leedale, G.F., Bradbury, P. (Eds.), An Illustrated Guide to the Protozoa, Organisms Traditionally Referred to as Protozoa, or Newly Discovered Groups, second ed. Society of Protozoologists, Lawrence, Kansas, pp. 371–656.

Maroteaux, L., Herzog, M., Soyer-Gobillard, M.O., 1985. Molecular organization of dinoflagellate ribosomal DNA: evolutionary implications of the deduced 5.8S rRNA secondary structure. Biosystems 18, 307–319.

Maupas, E., 1883. Contribution a l'etude morphologique et anatomique des infusoires ciliés. Arch. Zool. Exp. Gén. 1, 427–664.

Medlin, L.K., Elwood, H.J., Stickel, S., Sogin, M.L., 1988. The characterization of enzymatically amplified eukaryotic 16S-like rRNA-coding regions. Gene 71, 491–499.

Miao, M., Warren, A., Song, W., Wang, S., Shang, H., Chen, Z., 2008. Analysis of the internal transcribed spacer 2 (ITS2) region of scuticociliates and related taxa (Ciliophora, Oligohymenophorea) to infer their evolution and phylogeny. Protist 159, 519–533.

van Nues, R.W., Rientjes, J.M., van der Sande, C.A., Zerp, S.F., Sluiter, C., Venema, J., Planta, R.J., Raué, H.A., 1994. Separate structural elements within internal transcribed spacer 1 of *Saccharomyces cerevisiae* precursor ribosomal RNA direct the formation of 17S and 26S rRNA. Nucl. Acids Res. 22, 912–919.

Pan, H., Gao, F., Li, J., Lin, X., Al-Farraj, S.A., Al-Rasheid, K.A.S., 2010. Morphology and phylogeny of two new pleurostomatid ciliates, *Epiphyllum shenzhenense* n. sp. and *Loxophyllum spirellum* n. sp. (Protozoa, Ciliophora) from a mangrove wetland, South China. J. Eukaryot. Microbiol. 57, 421–428.

Pawlowski, J., 2000. Introduction to the molecular systematics of foraminifera. Micropaleontology 46 (Suppl. 1), 1–12.

Ponce-Gordo, F., Fonseca-Salamanca, F., Martínez-Díaz, R.A., 2011. Genetic heterogeneity in internal transcribed spacer genes of *Balantidium coli* (Litostomatea, Ciliophora). Protist 162, 774–794.

Posada, D., 2008. JModelTest: phylogenetic model averaging. Mol. Biol. Evol. 25, 1253–1256.

Retèl, J., Planta, R.J., 1967. Ribosomal precursor RNA in *Saccharomyces carlsbergensis*. Eur. J. Biochem. 3, 248–258.

Ronquist, F., Huelsenbeck, J.P., 2003. MrBayes 3: Bayesian phylogenetic inference under mixed models. Bioinformatics 19, 1572–1574.

von der Schulenburg, J.H.G., Englisch, U., Wägele, J.-W., 1999. Evolution of ITS1 rDNA in the Digenea (Platyhelminthes: Trematoda): 3′ end sequence conservation and its phylogenetic utility. J. Mol. Evol. 48, 2–12.

Schultz, J., Maisel, S., Gerlach, D., Müller, T., Wolf, M., 2005. A common core of secondary structure of the internal transcribed spacer 2 (ITS2) throughout the Eukaryota. RNA 11, 361–364.

Shimodaira, H., Hasegawa, M., 2001. CONSEL: for assessing the confidence of phylogenetic tree selection. Bioinformatics 17, 1246–1247.

Stamatakis, A., Hoover, P., Rougemont, J., 2008. A rapid bootstrap algorithm for the RAxML web-servers. Syst. Biol. 75, 758–771.

Stoeck, T., Bruemmer, F., Foissner, W., 2007. Evidence for local ciliate endemism in an Alpine anoxic lake. Microbiol. Ecol. 54, 478–486.

Strüder-Kypke, M.C., Wright, A.-D.G., Foissner, W., Chatzinotas, A., Lynn, D.H., 2006. Molecular phylogeny of litostome ciliates (Ciliophora, Litostomatea) with emphasis on free-living haptorian genera. Protist 157, 261–278.

Strüder-Kypke, M.C., Kornilova, O.A., Lynn, D.H., 2007. Phylogeny of trichostome ciliates (Ciliophora, Litostomatea) endosymbiotic in the Yakut horse (*Equus caballus*). Eur. J. Protistol. 43, 319–328.

Sun, P., Clamp, J.C., Xu, D., 2010. Analysis of the secondary structure of ITS transcripts in peritrich ciliates (Ciliophora, Oligohymenophorea): implications for structural evolution and phylogenetic reconstruction. Mol. Phylogenet. Evol. 56, 242–251.

Swofford, D.L., 2003. PAUP*. Phylogenetic Analysis using Parsimony (*and Other Methods). Version 4. Sinauer Associates, Inc., Sunderland (MA).

Vd'ačný, P., Foissner, W., 2008. Morphology, conjugation, and postconjugational reorganization of *Dileptus tirjakovae* n. sp. (Ciliophora, Haptoria). J. Eukaryot. Microbiol. 55, 436–447.

Vd'ačný, P., Foissner, W., 2009. Ontogenesis of *Dileptus terrenus* and *Pseudomonilicaryon brachyproboscis* (Ciliophora, Haptoria). J. Eukaryot. Microbiol. 56, 232–243.

Vd'ačný, P., Foissner, W., 2012. Monograph of the dileptids (Protista, Ciliophora, Rhynchostomatia). Denisia 31, 1–529.

Vd'ačný, P., Orsi, W., Foissner, W., 2010. Molecular and morphological evidence for a sister group relationship of the classes Armophorea and Litostomatea (Ciliophora, Intramacronucleata, Lamellicorticata infraphyl. nov.), with an account on basal haptorid litostomateans. Eur. J. Protistol. 46, 298–309.

Vd'ačný, P., Bourland, W.A., Orsi, W., Epstein, S.S., Foissner, W., 2011a. Phylogeny and classification of the Litostomatea (Protista, Ciliophora), with emphasis on free-living taxa and the 18S rRNA gene. Mol. Phylogenet. Evol. 59, 510–522.

Vd'ačný, P., Orsi, W., Bourland, W.A., Shimano, S., Epstein, S.S., Foissner, W., 2011b. Morphological and molecular phylogeny of dileptids: resolution at the base of the class Litostomatea (Ciliophora, Intramacronucleata). Eur. J. Protistol. 47, 295–313.

Visscher, J.P., 1923. Feeding reactions in the ciliate, *Dileptus gigas*, with special reference to the function of trichocysts. Biol. Bull. Mar. Biol. Lab. (Woods Hole) 45, 113–143.

Weisse, T., Strüder-Kypke, M.C., Berger, H., Foissner, W., 2008. Genetic, morphological, and ecological diversity of spatially separated clones of *Meseres corlissi* Petz & Foissner, 1992 (Ciliophora, Spirotrichea). J. Eukaryot. Microbiol. 55, 257–270.

Wolf, M., Achtziger, M.C., Schultz, J., Dandekar, T., Müller, T., 2005. Homology modeling revealed more than 20,000 rRNA internal transcribed spacer 2 (ITS2) secondary structures. RNA 11, 1616–1623.

Woodruff, L.L., Spencer, H., 1921. The food reactions of the infusorian *Spathidium spathula*. Proc. Soc. Exp. Biol. Med. 18, 183–184.

Woodruff, L.L., Spencer, H., 1922. Studies on *Spathidium spathula* I. The structure and behavior of *Spathidium*, with special reference to the capture and ingestion of its prey. J. Exp. Zool. 35, 189–205.

Wright, A.-D.G., Lynn, D.H., 1997a. Monophyly of the trichostome ciliates (Phylum Ciliophora: Class Litostomatea) tested using new 18S rRNA sequences from the vestibuliferids, *Isotricha intestinalis* and *Dasytricha ruminantium*, and the haptorian, *Didinium nasutum*. Eur. J. Protistol. 33, 305–315.

Wright, A.-D.G., Lynn, D.H., 1997b. Phylogenetic analysis of the rumen ciliate family Ophryoscolecidae based on 18S ribosomal RNA sequences, with new sequences from *Diplodinium*, *Eudiplodinium*, and *Ophryoscolex*. Can. J. Zool. 75, 963–970.

Wright, A.-D.G., Dehority, B.A., Lynn, D.H., 1997. Phylogeny of the rumen ciliates *Entodinium*, *Epidinium* and *Polyplastron* (Litostomatea: Entodiniomorphida) inferred from small subunit ribosomal RNA sequences. J. Eukaryot. Microbiol. 44, 61–67.

Wylezich, C., Meisterfeld, R., Meisterfeld, S., Schlegel, M.K., 2002. Phylogenetic analyses of small subunit ribosomal RNA coding regions reveal a monophyletic lineage of euglyphid testate amoebae (order Euglyphida). J. Eukaryot. Microbiol. 49, 108–118.

Xu, K., Foissner, W., 2005. Morphology, ontogenesis and encystment of a soil ciliate (Ciliophora, Haptorida), *Arcuospathidium cultriforme* (Penard, 1922), with models for the formation of the oral bulge, the ciliary patterns, and the evolution of the spathidiids. Protistology 4, 5–55.

Yi, Z., Chen, Z., Warren, A., Roberts, D., Al-Rasheid, K.A.S., Miao, M., Gao, S., Shao, C., Song, W., 2008. Molecular phylogeny of *Pseudokeronopsis* (Protozoa, Ciliophora, Urostylida), with reconsideration of three closely related species at inter- and intra-specific levels inferred from the small subunit ribosomal RNA gene and the ITS1-5.8S-ITS2 region sequences. J. Zool. 275, 268–275.

Zuker, M., 2003. Mfold web server for nucleic acid folding and hybridization prediction. Nucl. Acids Res. 31, 3406–3415.